Global Evaluation of Process Conditions and Corresponding Wave Modes in a Rotating Detonation Engine

Justin M. Weber[*], Kristyn B. Johnson[†], Wesley R. Boyette[‡], and Donald H. Ferguson[§]

National Energy Technology Laboratory - U.S. Department of Energy, Morgantown, WV, 26505

Rotating Detonation Engines (RDEs) show significant promise for enhancing the efficiency of gas turbine engines while maintaining low NO_x emissions. This work investigates the predictability of wave modes in a water-cooled RDE under varying operational conditions. Experimental data comprising over 6,700 samples was collected, including parameters such as flow rates, temperatures, pressures, and equivalence ratios. A machine learning approach using the XGBoost library was used to build a multi-class classifier, predicting wave modes based on these inputs. The model achieved a high accuracy of 97%, demonstrating that wave modes are not random but deterministic based on the process conditions. SHAP analysis was used to identify the most influential parameters affecting wave mode prediction. The results show that for the water-cooled NETL RDE, wave mode is determinant and predictable based on the process parameters.

I. Nomenclature

A	=	cross sectional area of the detonation channel [m^2]
D_{inner}	=	inner diameter of the detonation channel [m]
l_{cr}	=	critical fill height [m]
M	=	Molar mass of air and fuel mixture [kg kmol^{-1}]
$\dot{m}$	=	Total mass flow rate [kg s^{-1}]
$\dot{m}_{air,a}$	=	Air mass flow rate (FIC 0178) [kg s^{-1}]
$\dot{m}_{air,b}$	=	Air mass flow rate (FIC 0181) [kg s^{-1}]
$\dot{m}_{CH4}$	=	Methane mass flow rate [kg s^{-1}]
$\dot{m}_{H2}$	=	Hydrogen mass flow rate [kg s^{-1}]
$P_{air,header}$	=	Main air header pressure [kPa]
P_{back}	=	Back-pressure [kPa]
R	=	Ideal gas constant [kJ kmol^{-1} K^{-1}]
T_{air}	=	Air preheat temperature [K]
T_{fuel}	=	Fuel preheat temperature [K]
T_{mix}	=	Air and Fuel mixture temperature [K]
U_{cj}	=	Chapman–Jouguet wave speed [m s^{-1}]
U_w	=	Wave speed [m s^{-1}]
W_{count}	=	Wave count
ρ	=	Density of the air and fuel mixture [kg m^{-3}]
ϕ	=	Equivalence ratio

II. Introduction

Rotating detonation engines (RDEs) or rotating detonation combustors (RDC) have garnered significant interest from the US Department of Energy (US DOE) and other organizations due to their potential for stable hydrogen-air operation and their promise to enhance the thermodynamic efficiency of gas turbine engines while keeping NO_x

---
[*]National Energy Technology Laboratory - US DOE, and AIAA Member. Justin.Weber@netl.doe.gov
[†]National Energy Technology Laboratory - US DOE, and AIAA Member. kristyn.johnson@netl.doe.gov
[‡]National Energy Technology Laboratory - NETL Support Contractor, and AIAA Member. wesley.boyette@netl.doe.gov
[§]National Energy Technology Laboratory - US DOE, and AIAA Member. donald.ferguson@netl.doe.gov

emissions low [1]. Traditional gas turbine applications using hydrogen combustion face challenges due to instabilities like flashback and thermoacoustics. In contrast, RDEs leverage non-premixed reactants and short residence times within the combustor to maintain stable dynamic operation and low NO_x emissions [2].

Pressure gain combustion devices such as RDEs achieve pressure gain through an increase in total pressure. Although Kiel probes have been somewhat successful in measuring this total pressure [3], consistent evaluation remains difficult due to the harsh exhaust environment. The Equivalent Available Pressure (EAP) metric offers a means to estimate total pressure gain by assessing the flow's ability to perform work or generate thrust [4]. Experimental EAP characterization typically involves measuring thrust; however, coupling the combustor to a thrust stand is challenging for systems not in free movement, such as those with ducted exhausts. The "NPS Method" presents an alternative by using a static CTAP measurement upstream of the RDE exit plane, along with an assumed combustor Mach number and isentropic flow considerations, relying on choked (sonic) flow at the RDE exit [5].

At the RDE exit plane, strong circumferential variations in the flow field can cause simultaneous choked and unchoked flow [4]. These circumferential variations are dictated by the resulting wave mode, or the number of waves and what direction they are moving in the detonation channel. For effective coupling of an RDE to a conventional turbine, it is crucial to understand, predict, and measure their effects on turbine performance.

Previous work focused on studying wave mode transitions as the equivalence ratio was varied during a long duration tests in the NETL water-cooled RDE [6]. That work showed high correlation of the wave mode with process parameters, such as the equivalence ratio, suggesting that the RDE behavior is deterministic and can be reliably predicted.

This work takes a data analytics approach, with the primary objective to argue that the wave modes in RDEs are not random but are predictable based on operating conditions. This predictability can significantly impact the design and optimization of these engines. By varying conditions such as inlet air temperature, combustor back-pressure, mass flow rate, and equivalence ratio, different wave modes can be observed with both point measurement instrumentation and down-axis high speed imaging. This data set of over 6,700 samples will be used with a machine learning approach to identify the key process parameters, their influence on the wave mode, and the predictability of the wave mode.

III. Experimental Setup

Data presented throughout this work is collected during the operation of a water-cooled rotating detonation engine. Water-cooling enables long-duration tests by preventing excessive heating and thermal damage. Both the inner and outer walls of the engine are cooled using an open-loop, non-recycled water flow. The inlet and exit water temperatures for both the inner and outer walls are recorded, showing that exit water temperatures increase rapidly during the first 10 seconds of operation. It is assumed that once the exit water temperatures stabilize, the combustor has reached a thermally steady state. Although water-cooling allows indefinite operation without thermal damage, test runs are typically limited to 20 to 30 seconds to conserve hydrogen fuel while still achieving thermal stability in the test rig.

Figure 1 displays a cross-sectional diagram of the RDE installed in the Low Emission Combustor Test and Research (LECTR) facility at NETL. The detonation channel has an outer diameter of 14.88 cm and a width of 1.02 cm. A pintle-style injector is used, where hydrogen fuel is injected from the inner cavity through a series of 240 holes, each 0.076 cm in diameter, while air flows axially around the injector body. At the end of the channel, the flow area is decreased through an exit nozzle to choke the flow, which is then expanded through a diffuser to reduce unsteadiness. Following expansion through the diffuser, the products travel through water-cooled exhaust piping. Further downstream, a high-temperature control valve simulates the back pressure of a power turbine. Beyond the valve, the flow exits the building via an exhaust stack.

The post-combustor, a simple methane/air-fueled flame, is located just downstream of the diffuser, Figure 1. In addition to consuming any unburnt hydrogen so it doesn't travel downstream and burn in the stack, the flame serves as the ignition source for the RDE during start-up. Once the hydrogen reaches the torch, the combustion travels upstream to the injector, transitioning into detonation waves that travel around the detonation channel.

A. Instrumentation

A profile view of the pintle injector and combustion channel is shown in Figure 1(left). Six instrumentation modules are spaced around the combustor circumference at 60° intervals. As shown in Figure 1(right), the instrumentation modules are labeled A-F, each offering four axial instrumentation ports. Additional instrumentation and sampling locations are present along the diffuser section downstream of the RDE.

The six sampling ports accommodate various instruments, including capillary tube average pressure (CTAP) sensors, infinite tube pressure (ITP) sensors, fiber-based OH* chemiluminescence probes, ion probes, and thermocouples. An
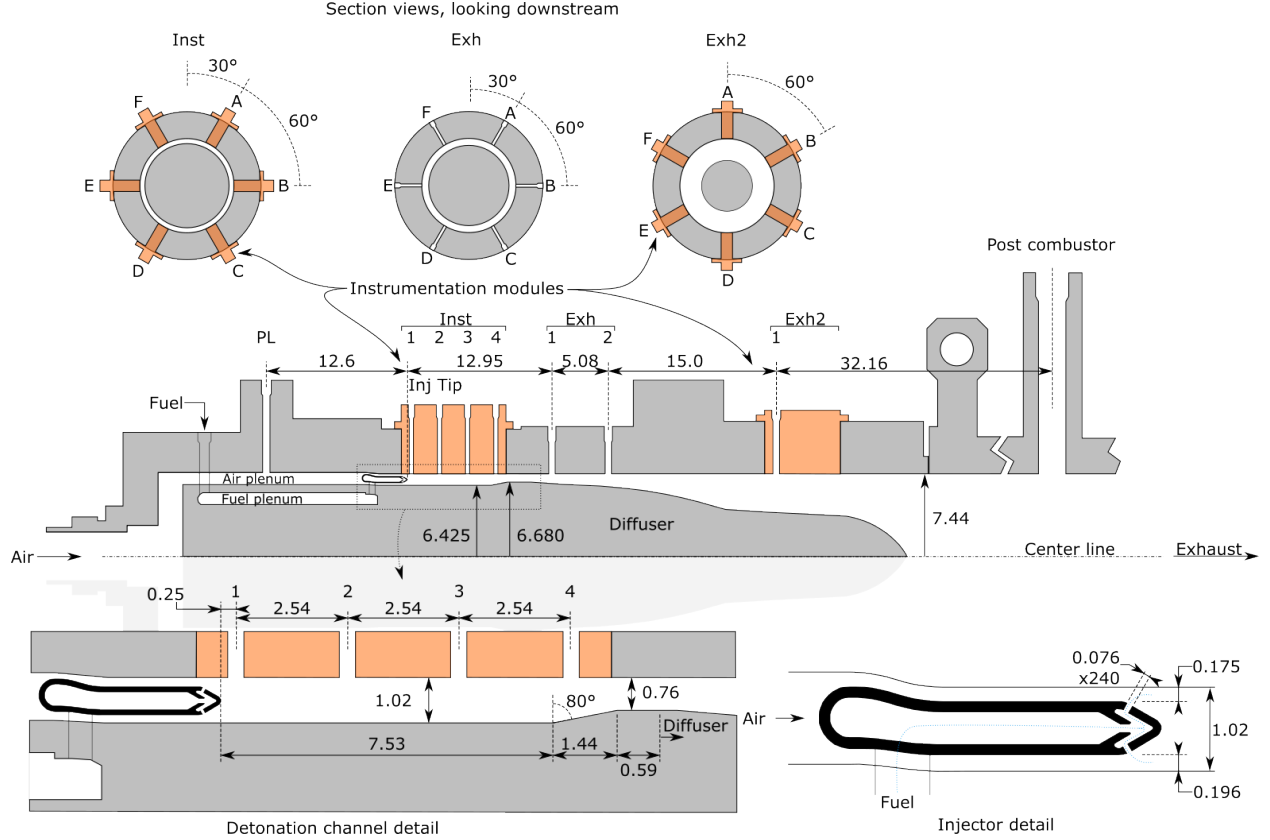
Fig. 1 Cross section view of the NETL water-cooled RDC with the pintle injector, showing the relative sizes of the plenums, details of the detonation channel, injector, and instrumentation port nomenclature. All dimensions in centimeters.

OH* chemiluminescence probe consists of a 1 mm sapphire fiber optic recessed approximately 2 mm from the outer wall of the RDE, providing an approximate 17° field of view relative to the inner wall of the combustion channel. The fiber optic is coupled to a 325 nm UV bandpass filter with a full width at half maximum (FWHM) of 110 nm, and a Hamamatsu R212 photomultiplier tube is used to capture the OH* chemiluminescence. Instrumentation data is recorded at various sampling rates of 1 MHz, 250 kHz, and 5 kHz using an NI PXI and LabVIEW interface. An Allen-Bradley process control system manages process variables such as fuel and air flow rates, combustion air inlet temperature, and back-pressure, with these conditions sampled at 1 Hz.

B. Imaging

High-speed OH* chemiluminescence images are captured through a window approximately 1.5 m downstream of the RDE exit plane. A Photron FASTCAM SAZ camera, equipped with an Invisible Vision UVI 2550-10-S25 intensifier, captures images at a frame rate of 60,000 frames per second. A Nikkor UV-105mm UV lens at the front of the intensifier captures light filtered through a UG11 325 nm bandpass filter with a FWHM of 110 nm, targeting OH* chemiluminescence. The intensifier's gate width capabilities limit image exposures to 14 μs, reducing pixel smearing from the spatial travel of detonation waves within a frame. The 512 x 512 pixel images provide a resolution of approximately 0.397 mm/pixel.

Due to the typical 20 to 30 second run times of the NETL RDE, continuously capturing high-speed images throughout the run is impractical because of limited on-board camera memory. Instead, a function generator sends a 5V pulse with a duty cycle of 3.5% at a frequency of 2 Hz, effectively triggering the camera to record 1024 images every 0.5 seconds. This provides a periodic sampling of the wave modes throughout the duration of the test.

IV. Data Analysis

The current data archive consists of 704 test runs of the pintle injector conducted from May of 2021 to March of 2023. The following process variables were varied over those test runs; the two main air flow rates ($\dot{m}_{air,a}$ and $\dot{m}_{air,b}$), hydrogen flow rate ($\dot{m}_{H2}$), methane flow rate ($\dot{m}_{CH4}$), air preheat temperature measured in the plenum (T_{air}), and back pressure (P_{back}). These process variables where changed to study the RDE at different equivalence ratios (ϕ), total mass flow rates ($\dot{m}$), back pressures (P_{back}), and preheat temperatures (T_{mix}).

In order to verify the predictability of wave modes in the NETL water-cooled RDE, systematic data treatment and analysis is applied. The following subsections will detail each step of the applied method, including image processing applied to high-speed images, temporal averaging of time series data, dataset generation and cleaning, and model creation.

A. Image Processing

A total of 13,071 imaging windows were recorded over the 704 test runs. An automated script was developed in Python to extract the wave count (W_{count}) and wave speed (U_w) from these images. This script performs the widely used detonation surface method and 2D FFT used in the RDE community to visualize the spatial and temporal movement of individual detonation waves [7]. The algorithm performs the following steps:

Circle identification To find the detonation channel in the images, a FFT is calculated for each pixel over the image stack. The height of the tallest peak in the FFT for each pixel is then extracted into a 2D array. Finally, a circle is fit to the top 2% of the peaks, identifying the detonation channel.

Detonation surface Based on the previously identified circle, a detonation surface is extracted by binning and averaging the pixels in 1°wedges around the circle for each frame. This results in a 2D array of pixel intensity as a function of detonation channel angle and time.

Wave count and speed A 2D FFT is calculated based on the detonation surface. The highest peak is identified, determining both the wave count and the wave frequency. Based on the wave count, frequency, and the physical dimensions of the RDE, a wave speed is calculated.

Fortunately, the wave modes observed in this RDE with the pintle injector are seldom counter rotating, allowing for this method to correctly identify the wave mode. The rotation direction is seemingly random and not consistent during individual tests. Due to this, wave direction is ignored. Further, No attempt was made to identify limit cycle oscillation (LCO) wave modes, which are present in the existing data [8].

B. Temporal Averaging

For each imaging window, a trigger signal is emitted and recorded by the NI PXI. This allows for calculation of process averages for the flow rates, temperatures, and pressures at each high-speed video segment. These averages, representing the conditions during each segment, were compiled into a comprehensive data set for subsequent analysis. Key metrics were then calculated for each period, including the Chapman-Jouguet wave speed (U_{cj}) using the SDToolBox [9]. Additionally, an FFT of the OH* chemiluminescence probe data is perform to extract the dominant frequency of the wave mode. This dominant frequency is a convoluted measurement of both the wave speed and wave count.

Most of the test runs where intentionally held at constant conditions throughout the duration of the 20 to 30 second test. However, for some tests, the mass flow rate of the fuel was intentionally varied [6]. This added sweeps of fuel mass flow rate that were sampled at 0.5 Hz, greatly expanding the condition samples. Unfortunately during these sweeps, both the total mass flow rate and equivalence ratio were varied, generating correlated variables.

C. Dataset Generation

By merging the image analysis with the temporal averaging, a comprehensive data set of 13,071 time averaged samples was generated. Additional variables were also created, derived from other measurements including the total mass flow rate ($\dot{m}$), which was calculated by summing the ($\dot{m}_{air,a}$ and $\dot{m}_{air,b}$), hydrogen flow rate ($\dot{m}_{H2}$), and methane flow rates ($\dot{m}_{CH4}$). Additionally, a mixture temperate (T_{mix}) is calculated by mixing the air flows at their temperature and the fuel flows at their temperatures using Cantera [10]. This mixture is also used to estimate the density of the mixture, using the pressure measured with the first CTAP (E1).

To ensure the consistency and reliability of the data, a self-consistency check was performed. This involved comparing the dominant frequency obtained from the OH* chemiluminescence probe with frequency derived from the wave speed and wave count extracted from the high-speed images, Figure 2. These two frequencies had to be within an
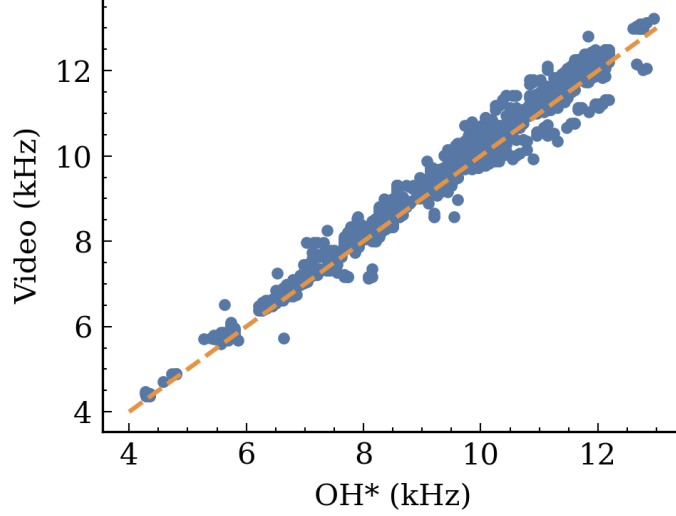
Fig. 2   Dominate frequency measured using the OH* chemiluminescence probe compared to the frequency extracted from the videos.

arbitrarily selected 1 kHz to be kept in the data set. Additionally, any wave speed that exceeded the calculated U_{cj} speed were removed form the dataset. This cleaning step was vital for verifying the accuracy of the measurements and the validity of the calculated metrics, identifying issues in the data where the automated processing of the images or the temporal data failed. There could be a number of reasons for this including data capture at startup or shutdown of the RDE, poor image quality, or catching a mode transition.

The cleaned data set consists of 6,702 samples with the wave modes ranging from 2 to 6 co-rotational waves. Total mass flow rates ($\dot{m}$) ranged from 0.5 to 0.85 kg/s, with equivalence ratios (ϕ) ranging from 0.13 to 1. Mixture temperature of the air and fuel streams (T_{mix}) ranging from 376 to 466 K with the back pressures (P_{back}) ranging from 117.2 kPa to 474.2 kPa, absolute. These ranges along with mean, standard deviation, and 25, 50, and 75% quartiles are provided in Table 1.

Table 1   Dataset statistics.

	P_{back} (kPa [abs])	$\dot{m}$ (kg/s)	ϕ	T_{mix} (K)
mean	196.3	0.681	0.667	436
std	70.2	0.088	0.159	17
min	117.2	0.507	0.133	376
25%	142.6	0.616	0.493	419
50%	161.7	0.693	0.649	442
75%	246.8	0.744	0.785	449
max	474.2	0.846	1.040	466

To visualize the relationships of the input parameters and the wave count, a pairwise plot is shown in Figure 3. In the pairwise format, the four input parameters and wave count are represented on both the x- and y-axes. Subplots to the lower left of the diagonal contain all possible 2D scatter plots between the five variables, each with a linear fit overlaid as an orange dashed line. Along the diagonal (top-left to bottom-right) where variables are self-aligned, normalized histograms visualize variable distribution. Above the diagonal, 2D histogram contours highlight sampling densities for each variable combination.

It is apparent that the mixture temperature (T_{mix}) is correlated with the back pressure, mass flow rate, and equivalence ratio. In addition, there are strong relationships between the total mass flow rate, the equivalence ratio, and the mixture

temperature with the wave count. As the total mass flow rate increases, so does the wave count. The equivalence ratio shows an inverse relationship with the wave count. Finally, as the temperature increases, so does the wave count.
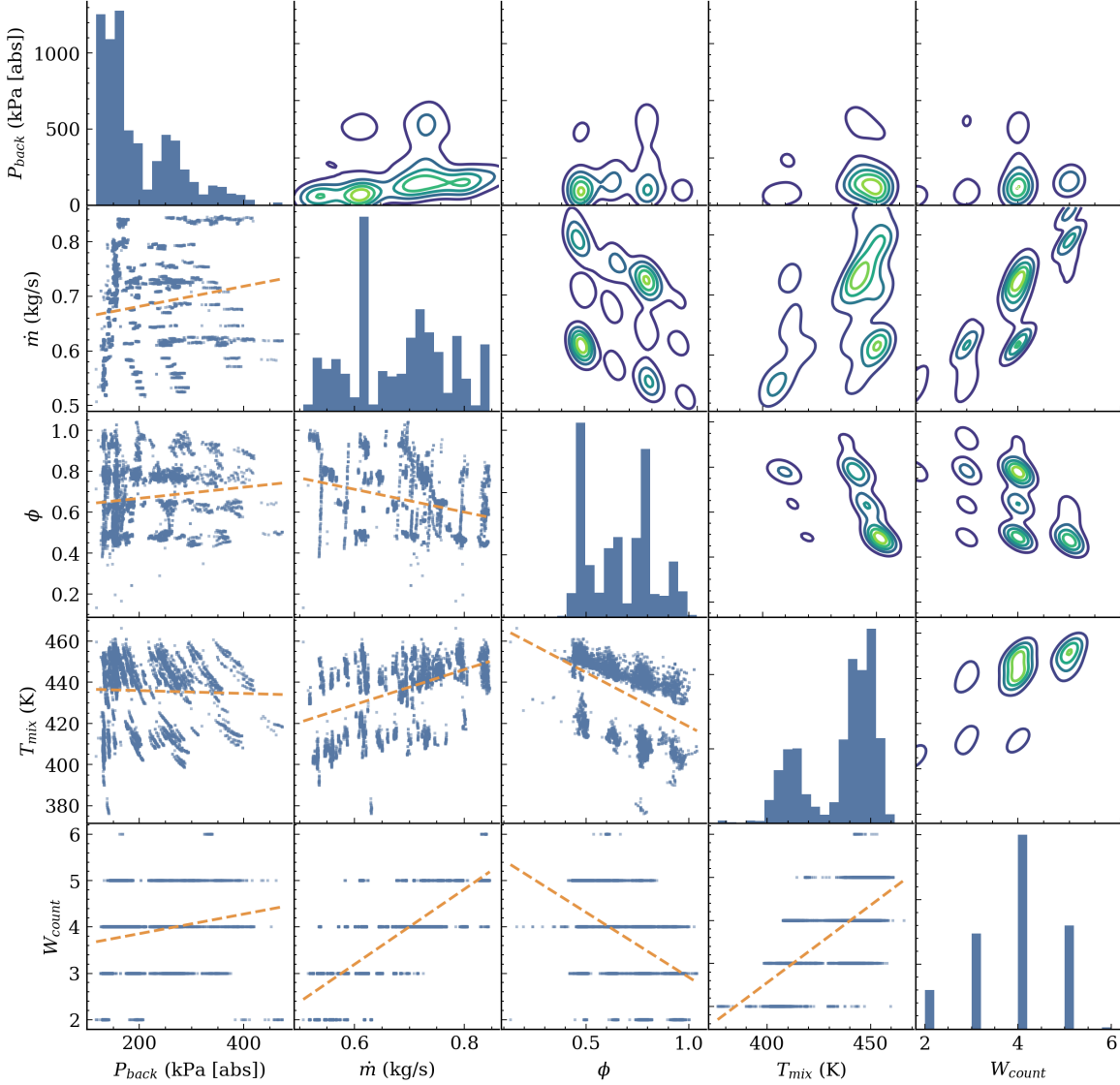

Fig. 3 Pairwise plot of selected input parameters (P_{back}, $\dot{m}$, ϕ, T_{mix}) and the output parameter (W_{count}). Lower triangle is scatter plots with a linear fit of the two variables. Diagonal are histograms of the variable. Upper triangle are contours of the 2D histogram.

D. Classifier Model

Once the data set was verified for consistency, the XGBoost library was used to build a gradient boosted multi-class classifier [11]. The library utilizes decision tree ensembles, consisting of a set of classification and regression trees. Decision tree learning is a broadly used and proven supervised learning approach, which can be trained on datasets with known input-output pairs. Within a the tree structure, internal nodes correspond to input features, branches correspond to rules or weighted mathematical functions applied to upstream data, and leaves represent the output of the algorithm. The depth of the tree, representing the maximum path length from the root to the leaf, impacts the complexity of the tree. Shallow trees may under-fit data, while deeper trees may over-fit data. A tree ensemble combines the prediction scores of multiple simple decision trees. The unique approach of a gradient boosted decision tree lies in its incremental construction of the ensemble. At each iteration, a new decision tree is trained on the error of the base ensemble, which

is then "added" to the base ensemble with a negative sign, reducing error of the cumulative ensemble. This process is repeated until a desired training threshold is met.

The inputs to this classifier were the averaged process conditions, and the output was the wave mode. Given that no counter-rotating wave modes were observed with the pintle injector, the output was simplified to only the wave count with the following five classes; 2, 3, 4, 5, or 6.

The model development effort started using all 16 measured input process parameters. However, as alluded to in section IV.C, through a trial and error process and combining similar parameters, these input parameters were reduced to 4, while maintaining model accuracy. The four input parameters that the final model was trained on were the back pressure (P_{back}), total mass flow rate ($\dot{m}$), equivalence ratio (ϕ), and the air and fuel mixture temperature (T_{mix}).

To avoid over-fitting of the data, several XGBoost hyper parameters were tuned. These parameters included
- maximum tree depth which was reduced to 3 to limit the model complexity.
- Minimum child weight increased to 3 to require more observations per leaf
- Gamma set to 1 to require stronger evidence for additional splits
- Subsample rate of 0.8 randomly selects 80% of data for each tree
- Column sampling of 0.8 uses 80% of features per tree
- Learning rate reduced to 0.1 for more conservative updates.

These settings proved to help prevent the model from simply memorizing the data.

V. Discussion

The objective of this analysis is to prove that for the NETL RDE with pintle injector, wave modes are deterministic and not random. Further, these wave modes are predictable based solely on the input conditions, namely the flow rates, temperatures, and pressures.

A. Model Performance

Overall, the model performs well at predicting the wave counts. For model validation, 30% of the data (2,011 samples) was randomly removed before training for a cross-validation data set. This approach allowed for an assessment of the model's performance on unseen data, testing its generalization. The model achieved an accuracy of 97% on the training data and achieved an impressive accuracy of 96% on the validation data, indicating its reliability in predicting the wave count based solely on the four process conditions. This also shows that the model does not simply memorize the input data.

To further assess the performance of the model, a confusion matrix was constructed, which clearly demonstrates the accurate predictive capability of the model on the cross-validation data, Figure 4. Each cell in the confusion matrix represented the count of true versus predicted wave counts, providing a comprehensive visualization of the model's effectiveness and any misclassifications. Across all of the classes, the model accurately predicts the wave counts, with the 6 wave mode being most accurate at 100% and the 5 wave count being the lowest at 94%. The model has the highest count of misclassifications between the 4 predicted waves and 5 true waves. This is also where a majority of the samples are located and an area where LCO behavior typically occurs [8].

B. Operational Maps

The model can be used to generate predictive operational maps over the input parameters. For example, at a mixture temperature of $T_{mix} = 400K$ and back pressure of $P_{back} = 120$ kPa, the wave counts can be predicted over a range of equivalence ratios and mass flow rates, Figure 5. This specific operation map shows how increases in mass flow rate from 0.5 to 0.85 kg/s at a fixed equivalence ratio increases the wave count from 2 to 4 waves. The model struggles with predictions at a mass flow rate of 0.85 kg/s, due to a lack in data density at the higher mass flow rates.

This predictive model can now be used for several purposes including process models or other models that require a wave count as input as well as model validation of computational fluid dynamic models. Another intriguing use case is for autonomous discovery where experimental test campaigns can be planned to focus on the transitional areas. The model can be used to predict these transitional conditions, generating a list of process conditions to evaluate. This will allow for better defined operational maps and could elicit explanations for these modal transitions.
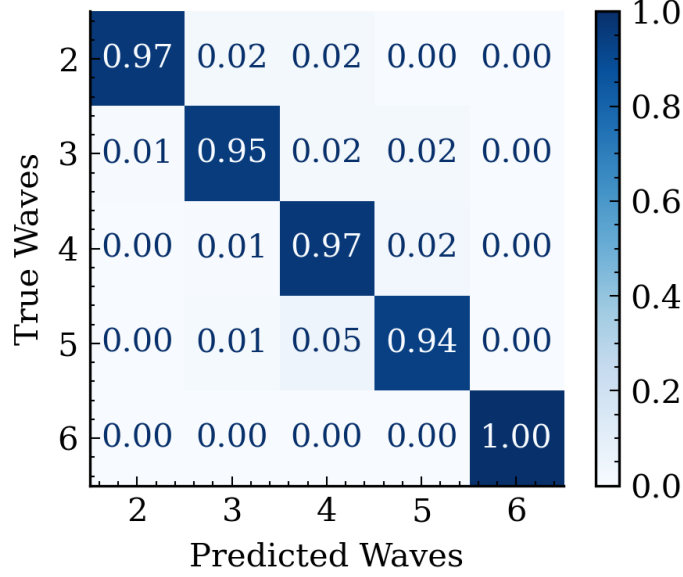
Fig. 4 Confusion matrix, comparing the predicted wave counts to the measured wave counts for the cross-validation data, normalized by the true counts (rows).
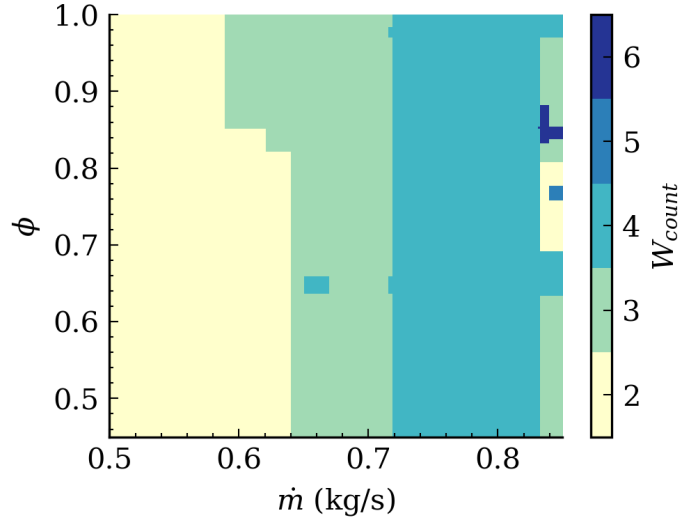

Fig. 5 Model predicted operational map at mass flow rates ($\dot{m}$) ranging from 0.5 to 0.85 kg/s and equivalence ratios ranging from 0.45 to 1, at T_{mix} = 400K and P_{back} = 120 kPa.

C. Parameter Importance

The model can also be used to determine the most influential input parameters on the wave count. Using XGBoost's F score metric a global indicator of the influence of a parameter can be assessed. For this model, the total mass flow rate ($\dot{m}$) is the most influential input parameter, Figure 6. This is followed by the back pressure (P_{back}), with the mixture temperature (T_{mix}) and equivalence ratio (ϕ) tying for last. However, this metric does not explain how changing the input parameter effects the wave count.

To understand the contributions of the input variables on the model's predictions, SHAP (SHapley Additive exPlanations) analysis technique was employed[12]. SHAP values offer a unified measure of feature importance, providing a detailed breakdown of how changes in the input variables influenced the predicted wave count, offering valuable insights into the underlying influences.

The SHAP summary lists the relative order of importance of the variables, along with the impact of the characteristic
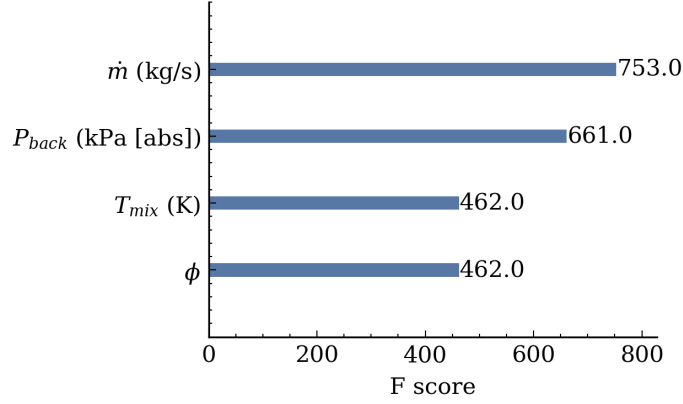
8

Fig. 6   F score of the model input parameters.
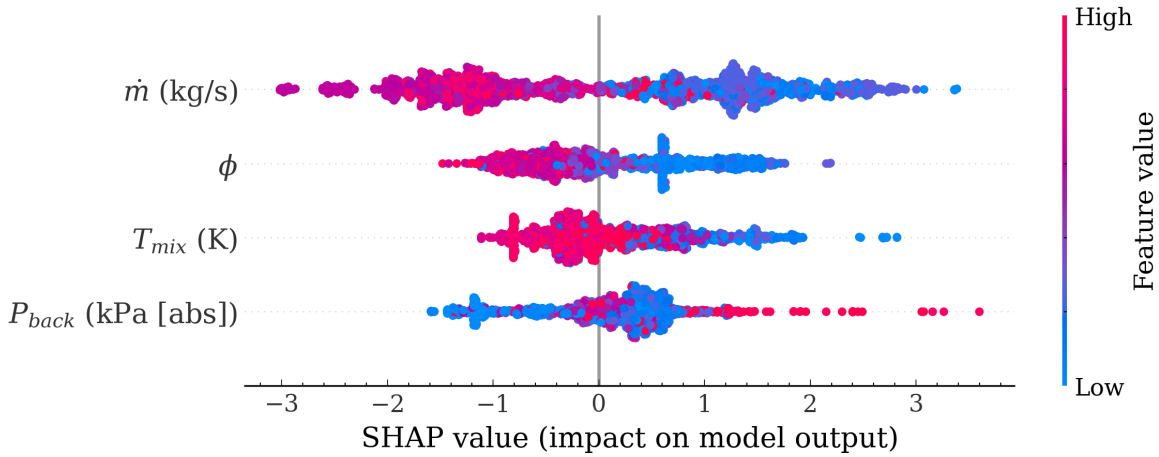

Fig. 7   SHAP summary plot showing the impact of input variables on the predicted wave count. Each point represents a SHAP value for a specific feature and instance, illustrating the distribution of feature importance.

values on the SHAP value for all model training data, Figure 7. Based on the mean SHAP value, the most impactful input variable is again the total mass flow rate ($\dot{m}$). The rest of the order is slightly different, with the equivalence ratio (ϕ) coming next followed by the mixture temperature (T_{mix}) and finally the back pressure (P_{back}). The mean SHAP value emphasizes the average impact of the variable on the output, minimizing the effect of the extremes.

The SHAP summary also indicates the effect of the relative feature value on the wave count. However, here the impact of the mass flow rate on the model output (wave count) does not agree with the relationship displayed in Figure 3. The SHAP values indicate that as the $\dot{m}$ increases, the wave count should decrease. While the relationship displayed in Figure 3 clearly indicates that as the $\dot{m}$ increases, so does the wave count. It is unclear if the multi classification of the wave count is causing this inconsistency in the SHAP values.

The rest of the SHAP values do make sense and agree with the relationships presented in Figure 3. As the equivalence ratio (ϕ) increases, the wave count decreases. Similarly, as the mixture temperature (T_{mix}) increases, the wave count decreases. Finally, as the back pressure (P_{back}) increases, so does the wave count.

D. Wave Speed

The measured wave speeds were compared to the theoretical Chapman-Jouguet wave speed (U_{cj}). The measured wave speeds ranged from 57% to 74% of U_{cj} for 90% of the data points (between 5th and 95th percentiles), Figure 8. This indicates that the actual detonation wave speeds are generally lower than the theoretical maximum, as expected in practical, non-ideal conditions. This suggests that it will be difficult to predict wave speeds with simple relationships.

Further, the wave speeds are strongly influenced by the resulting wave mode and equivalence ratio, ϕ, Figure 9. As
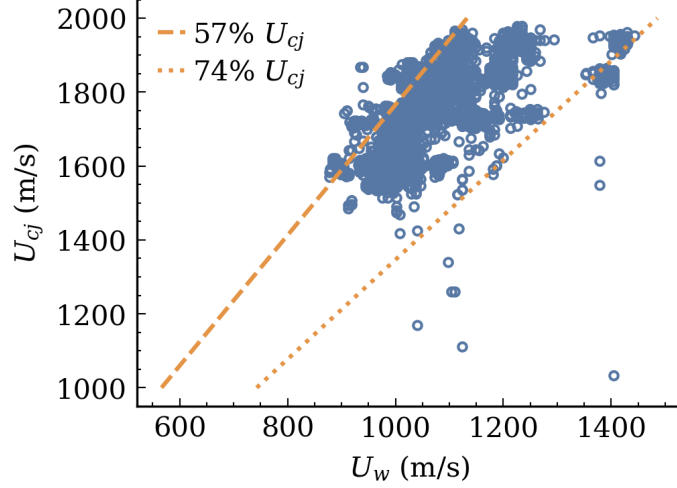
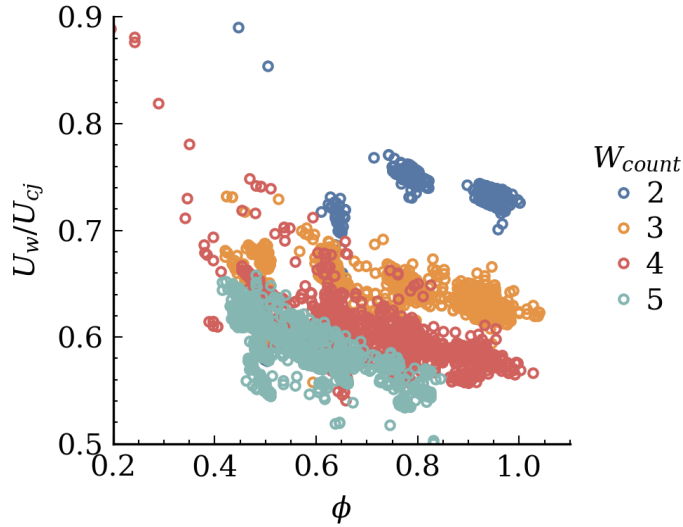**Fig. 8 Measured wave speed compared to the CJ speed.**

Fig. 9 Measured wave speed normalized by U_{cj} as a function of equivalence ratio, colored by wave count.

expected, as the equivalence ratio increases, the wave speed increases. At certain process conditions, the wave mode changes. Typically, when the wave count decreases, significant increases in wave speed are observed. Interestingly, as the wave count decreases, the wave speed is closer to the theoretical CJ speed. Also, at lower equivalence ratios, the wave speed is closer to the theoretical CJ speed. It cannot be concluded that this relationship is solely based on the wave count, because at one set of process conditions the same wave count is observed. It takes a different set of process conditions to change the wave count.

E. Simple Model

The relationships between the variables agree with the trends predicted by the wave count model proposed by Wolański[13], where t_t is the time it takes for a single wave to traverse the detonation channel and t_f is the time it takes to fill the detonation channel to some critical length, l_{cr}, Equation 1.

$$W_{count} = \frac{t_t}{t_f} \tag{1}$$

The traverse time, t_t, can be expressed as the circumference of the detonation channel divided by the wave speed, Equation 2.

$$t_t = \frac{\pi D_{inner}}{U_w} \tag{2}$$

Where D_{inner} is the inner diameter. The fill time, t_f, can be defined as the fill volume, divided by the volumetric flow rate of the air and fuel, Equation 3.

$$t_f = \frac{A l_{cr}}{\dot{m}/\rho} \tag{3}$$

Where A is the cross sectional area of the detonation channel, ρ is the density of the air and fuel mixture at T_{mix} and pressure P_{back}. By re-arranging these equations and assuming the ideal gas law, we see the three parameters that the XGBoost model settled on, Equation 4. The forth parameter, ϕ, is embedded in the wave speed.

$$W_{count} = \frac{\pi D_{inner} \dot{m} R T_{mix}}{U_w A l_{cr} P_{back} M} \tag{4}$$

Where R is the ideal gas constant and M is the molar mass of the air fuel mixture. According to Equation 4, as the mass flow rate ($\dot{m}$) and mixture temperature (T_{mix}) increases, so does the wave count. This relationship agrees with the data presented in Figure 3. Additionally, as the equivalence ratio increases, increasing the wave speed (U_w) the wave count decreases, agreeing with the results in Figure 3. Unfortunately, the pressure is not as clear, because the pressure effects both the fill time and the wave speed simultaneously. Finally, an attempt to solve for the critical length, l_{cr}, was made but it did not turn out to be a scalar or a clear function of the process variables.

VI. Conclusion

A total of 704 test runs of the hydrogen fueled pintle injector RDE were performed. By sub-processing these test runs every 0.5 seconds when high speed images a periodically captured, a total dataset of 13,071 samples is assembled using automated data processing scripts. Through data quality and self consistency checks, this data set is reduced to 6,702 samples.

An XGBoost multi-class classifier model was fit to the data set to predict the wave mode (2, 3, 4, 5, or 6 waves) based on only four input parameters, capturing the process conditions. These parameters include the back pressure (P_{back}), total mass flow rate ($\dot{m}$), equivalence ratio (ϕ), and the air and fuel mixture temperature (T_{mix}). The classification model achieved an accuracy of 97%.

The effectiveness of the XGBoost model demonstrates the predictability of wave modes in the NETL RDE with the pintle injector. The wave modes are deterministic, and can be predicted using a machine learning model based solely on four input parameters describing the operating conditions. This suggests that wave modes are not random and are dictated by the boundary conditions of the RDE. These boundary conditions consist of the process conditions, walls, and geometry of the RDE.

The insights gained from this study provide a robust foundation for further research and optimization of RDEs. Future work will focus on expanding the simple model into a mechanistic model to further elucidate the relationships of the process parameters on the wave mode.

Disclaimer

This project was funded by the United States Department of Energy, National Energy Technology Laboratory. Neither the United States Government nor any agency thereof, nor any of their employees, nor the support contractor, nor any of their employees, makes any warranty, express or implied, or assumes any legal liability or responsibility for the accuracy, completeness, or usefulness of any information, apparatus, product, or process disclosed, or represents

that its use would not infringe privately owned rights. Reference herein to any specific commercial product, process, or service by trade name, trademark, manufacturer, or otherwise does not necessarily constitute or imply its endorsement, recommendation, or favoring by the United States Government or any agency thereof. The views and opinions of authors expressed herein do not necessarily state or reflect those of the United States Government or any agency thereof.

References

[1] Sousa, J., Paniagua, G., and Collado Morata, E., "Thermodynamic analysis of a gas turbine engine with a rotating detonation combustor," *Applied Energy*, Vol. 195, 2017, pp. 247–256. https://doi.org/10.1016/j.apenergy.2017.03.045.

[2] Ferguson, D. H., O'Meara, B., Roy, A., and Johnson, K., "Experimental measurements of NOx emissions in a Rotating Detonation Engine," *AIAA Scitech 2020 Forum*, American Institute of Aeronautics and Astronautics, ORlando, FL, 2020. https://doi.org/10.2514/6.2020-0204, URL https://arc.aiaa.org/doi/10.2514/6.2020-0204.

[3] Bach, E., Stathopoulos, P., Paschereit, C. O., and Bohon, M. D., "Performance analysis of a rotating detonation combustor based on stagnation pressure measurements," *Combustion and Flame*, Vol. 217, 2020, pp. 21–36. https://doi.org/10.1016/j.combustflame.2020.03.017.

[4] Kaemming, T. A., and Paxson, D. E., *Determining the Pressure Gain of Pressure Gain Combustion*, AIAA, 2018. https://doi.org/10.2514/6.2018-4567, URL https://arc.aiaa.org/doi/abs/10.2514/6.2018-4567.

[5] Brophy, C. M., and Codoni, J. R., "Experimental Performance Characterization of an RDE Using Equivalent Available Pressure," *AIAA Propulsion and Energy 2019 Forum*, Indianapolis, IN, 2019. https://doi.org/10.2514/6.2019-4212.

[6] Boyette, W. R., Bedick, C., Weber, J., and Ferguson, D. H., "Equivalence Ratio Scans in a Rotating Detonation Engine," *AIAA SCITECH 2024 Forum*, 2024. https://doi.org/10.2514/6.2024-2793.

[7] Bennewitz, J. W., Bigler, B. R., Schumaker, S. A., and Hargus, W. A., "Automated image processing method to quantify rotating detonation wave behavior," *Review of Scientific Instruments*, Vol. 90, No. 6, 2018, p. 065106. https://doi.org/10.1063/1.5067256.

[8] Johnson May, K. B., Weber, J., Ferguson, D., Nix, A., and Sidwell, T. G., "Limit Cycle Oscillating Detonation Wave Behavior Analysis Within a Rotating Detonation Engine," *Journal of Propulsion and Power*, Vol. 40, No. 5, 2024, pp. 701–716. https://doi.org/10.2514/1.B39271, URL https://doi.org/10.2514/1.B39271.

[9] Browne, S. T., Ziegler, J. L., Bitter, N. P., Schmidt, B. E., Lawson, J., and Shepherd, J. E., *SDToolbox: Numerical Solution Methods for Shock and Detonation Jump Conditions*, Pasadena, CA, 1 2023.

[10] Goodwin, D. G., Moffat, H. K., Schoegl, I., Speth, R. L., and Weber, B. W., "Cantera: An Object-oriented Software Toolkit for Chemical Kinetics, Thermodynamics, and Transport Processes," https://www.cantera.org, 2023. https://doi.org/10.5281/zenodo.8137090, version 3.0.0.

[11] Chen, T., and Guestrin, C., "XGBoost: A Scalable Tree Boosting System," *Proceedings of the 22nd ACM SIGKDD International Conference on Knowledge Discovery and Data Mining*, ACM, New York, NY, USA, 2016, pp. 785–794. https://doi.org/10.1145/2939672.2939785, URL http://doi.acm.org/10.1145/2939672.2939785.

[12] Lundberg, S. M., and Lee, S.-I., "A Unified Approach to Interpreting Model Predictions," *Advances in Neural Information Processing Systems 30*, edited by I. Guyon, U. V. Luxburg, S. Bengio, H. Wallach, R. Fergus, S. Vishwanathan, and R. Garnett, Curran Associates, Inc., 2017, pp. 4765–4774. URL http://papers.nips.cc/paper/7062-a-unified-approach-to-interpreting-model-predictions.pdf.

[13] Wolański, P., "Rotating detonation wave stability," *23rd international colloquium on the dynamics of explosions and reactive systems*, 2011, pp. 1–6.